DSMC-PIC Analysis of a Plume from a Small Ion Engine* †

Michio Nishida
Department of Aeronautics and Astronautics, Kyushu University
Fukuoka 812-8581, Japan
nishida@aero.kyushu-u.ac.jp

Toru Hyakutake
Department of Mechanical Engineering, Okayama University
Okayama 700-8530, Japan
hyaku@mech.okayama-u.ac.jp

Hitoshi Kuninaka and Kyoichiro Toki
Institute of Space and Astronautical Science
Sagamihara, Kanagawa 229-8510, Japan
kuninaka@newslan.isas.ac.jp
toki@newslan.isas.ac.jp

IEPC-01-110

This paper describes the numerical studies of a plume exhausted from a small size ion thruster, especially focusing on the behavior of charge-exchange (CEX) ions which strike the surface of the ion thruster to give damage on it. The numerical simulation uses the DSMC-PIC method. The conditions specified for the small ion thruster are the beam current of 7.7 mA, beam voltage of 1,000 V and mass flow rate of 0.05 mg/s. The diameter of the ion thruster is 20 mm. The numerical results are compared with the experiments to give physical explanation of the experimental results.

Introduction

The Institute of Space and Astronautical Science (ISAS) is promoting the sample and return space mission from an asteroid, the MUSES-C, which is scheduled to be launched in 2002 and to bring back some specimens to the Earth in 2007 from 1998SF36 [1]. In the MUSES-C mission, a cathode-less microwave discharge ion engine system with Xenon as propellant is ready as a primary propulsion. The angle of the ion beam spread and the plume contamination by backflow are concerns for the equipment of an ion engine. An ion thruster plume is composed of beam ions and neutral atoms. Within the plume, the neutral atoms with thermal velocities collide with highly energetic beam ions, which causes a charge-exchange reaction as follows:

$$Xe^{+}_{fast} + Xe_{slow} \rightarrow Xe^{+}_{slow} + Xe_{fast} \qquad (1)$$

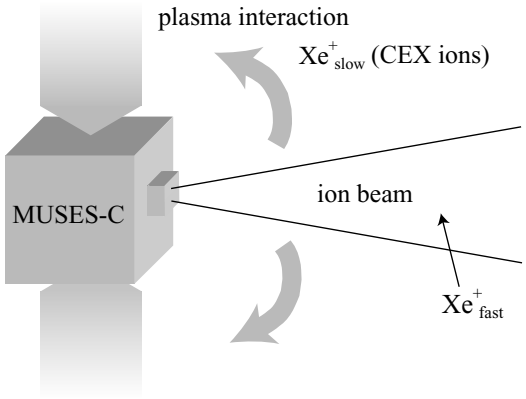

Figure 1. Plasma interaction of ion thruster plume.

This process generates fast neutral atoms and slow ions with a thermal speed, which is called CEX (charge-exchange) ions. These slow CEX ions are scattered outwards and interact with the surface on a spacecraft (Fig. 1). Therefore, it is necessary to reveal the behavior of the CEX ions which strike the surface behind the

*Presented as Paper IEPC-01-110 at the 27th International Electric Propulsion Conference, Pasadena, CA, 15-19 October, 2001.

ion thruster to give damage on it, because the ion engines which are equipped with the MUSES-C spacecraft are used for a long term. At ISAS, the experimental simulation using a small size ion thruster was carried out in order to examine the plume contamination from the MUSES-C ion thruster [2]. In the present work, the structure of the plume from the small ion thruster is numerically re-constructed and the behavior of the CEX ions is revealed to give physical explanation of the experimental results.

Studies of ion thruster plume contamination have been numerically conducted for several years [3]-[9]. Samanta Roy et al. [3]-[5] employed the PIC method [6] to investigate the structure of an ion thruster plume. Wang et al. carried out a 3-D simulation of the ion thruster by using the PIC-MCC model [7], [8]. In these studies, an analytical model was used to estimate the neutral density field. On the other hand, van Gilder et al. simultaneously treated both neutral atoms and ions as particles, and calculated the UK-10 ion thruster plume by using the DSMC-PIC method [9]. The velocity distribution of neutral atoms is better represented by the DSMC-PIC method than the method of Roy and Wang. However, it is apparent that the DSMC-PIC method increases computational time much more than the method that handles only ions. In the present study, the neutral atom density and velocity distributions are calculated beforehand by using the DSMC method [10], then the motions of ions are analyzed by the DSMC-PIC method. The CEX ion density is generated based on the spatial volumetric production rate of the CEX ions.

Operating conditions for the small size ion thruster are shown in Table 1, where the conditions for the MUSES-C ion thruster are also given for reference. The neutral atom density at the exit of the small ion thruster calculated based on these parameters is 9.5×10^{18} m^{-3}, and the ion density is 1.0×10^{16} m^{-3}. Therefore, the propellant utilization efficiencies for the small ion thruster is low, approximately 20 %. It is predicted that the amount of the CEX ion from the small ion thruster is much larger than that from the MUSES-C ion engine.

Numerical Methods

The computational domain is shown in Fig. 2 which is divided into 4,200 cells. The flow model we consider is axisymmetric, and the backflow region is added to capture the trajectory of the CEX ions that reach this region. Sonic conditions for the neutral atoms are assumed at the ion thruster exit. In the present study, the density and velocity of neutral atoms are calculated beforehand using the DSMC method. Secondly, using the DSMC-PIC method simulates the motion of ions. A

Table 1. Ion thruster conditions (A: a small ion thruster, B: MUSES-C ion thruster)

ion thruster conditions	A	B
propellant	Xe	Xe
thrust (mN)	0.4	8
mass flow (mg/s)	0.0487	0.21
beam voltage (V)	1000	1500
beam current (A)	0.0077	0.14
diameter of ion thruster (mm)	20	105

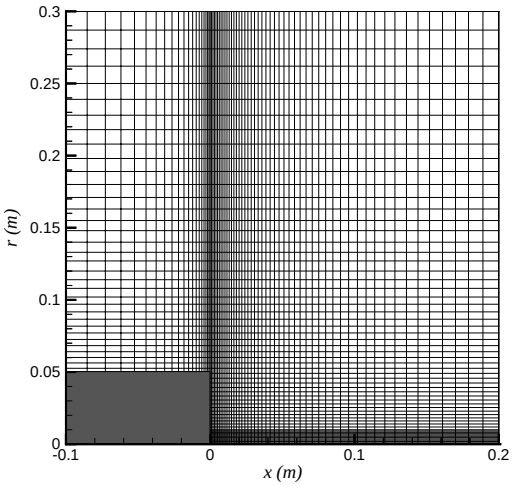

Figure 2. Computational grid.

Gaussian distribution gives the current density at the thruster exit plane. The angle of the beam spread at the exit is considered to be in the range from $\alpha = 5°$ to 30°. The exit conditoins for the small ion thruster are summarized in Table 2, which are used as boundary conditions in the present computations. Generally, a neutralizer is equipped with an ion engine, so that it is necessary to treat electrons emitted from it. However, it is assumed for a simple analysis that electron density is distributed according to the Boltzmann relation:

$$n_{\mathrm{e}} = n_{\mathrm{o}} \exp(e\Phi / kT_{\mathrm{e}}) \tag{2}$$

where n_{e} is the electron density, n_{o} is the plasma density at reference, e is the electronic charge, Φ is the potential, k is the Boltzmann constant and T_{e} is the electron temperature. The plasma in the plume is assumed to be quasineutral ($n_{\mathrm{i}} \approx n_{\mathrm{e}}$), so that the plasma potential can be determined by applying ion density (n_{i}) and electron temperature (T_{e}) to Eq. (2). Hence, it is not necessary to solve the Poisson's equation. Experiments of the small ion thruster at ISAS show $T_{\mathrm{e}} = 1.0 - 5.0$ eV in the ion beam. Therefore, two values of the electron temperature, 1.0 and 5.0 eV, are chosen in the present simulation.

Table 2. Exit conditions of a small ion thruster

neutral atom density	9.5×10^{18} m^{-3}
ion density	1.0×10^{16} m^{-3}
neutral atom velocity	230 m/s
ion velocity	38 km/s

Charge exchange reaction occurs in the ion beam as shown in Eq.(1), and the production rate of the CEX ions is given by

$$\dot{n}_{\rm cex} = n_{\rm n} n_{\rm i} v_{\rm r} \sigma_{\rm cex}(v_{\rm i}) \tag{3}$$

where $n_{\rm n}$ is the neutral atom density, $n_{\rm i}$ is the ion density, $v_{\rm r}$ is the relative velocity between neutral atoms and ions, and $\sigma_{\rm cex}$ is the charge exchange cross section given by Rapp and Francis [11].

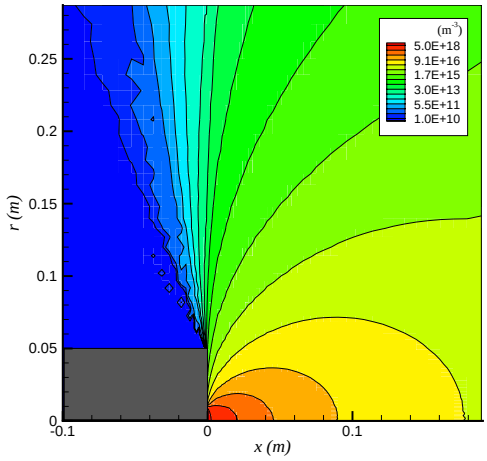

Figure 3. Number density contours of Xe neutral atoms.

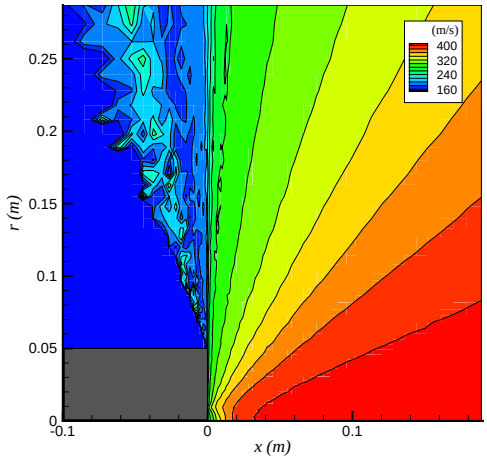

Figure 4. Velocity contours of Xe neutral atoms.

Results and Discussion

First of all, the simulation of a neutral plume from the ion thruster was carried out by using the DSMC method. In Figs. 3 and 4, the number density and velocity contours of neutral atoms are shown. There are a small number of particles which arrive in the backflow region. Thus determined density and velocity of neutral atoms are employed in the simulation of ions. A forecollision velocity of neutral atoms gives a postcollision ion velocity produced by the charge exchange reaction.

In order to determine the angle of the ion beam divergence α at the thruster exit, the results computed for various angles are compared with the experimental data. Comparisons of the computed and measured on-axis total ion flux for $T_{\rm e} = 1.0$ eV are presented in Fig. 5. As shown in this figure, the computed results at $\alpha = 20°$ agree quite well with the experiments. In the case of $T_{\rm e} = 5.0$ eV, a good agreement between the computa-

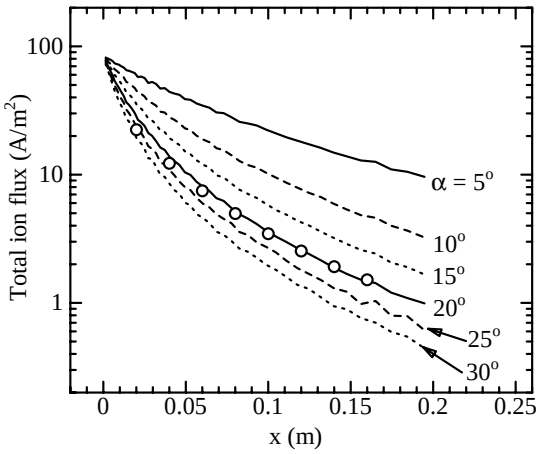

Figure 5. Comparisons of Xe ion flux on the axis.

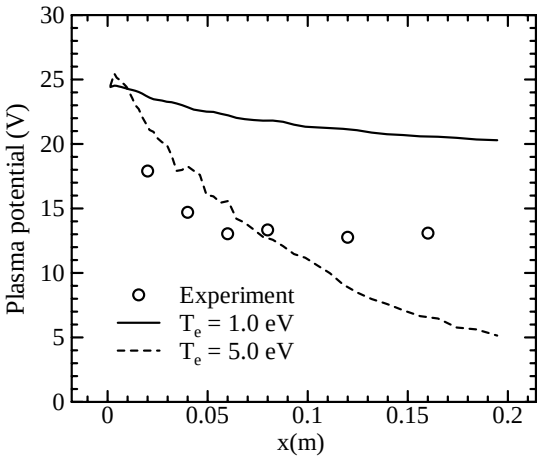

Figure 6. Comparisons of plasma potential on the axis.

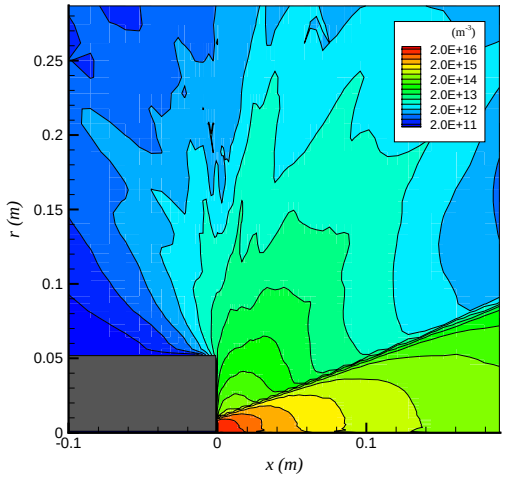

Figure 7. Ion density contours for $T_e = 1.0$ eV.

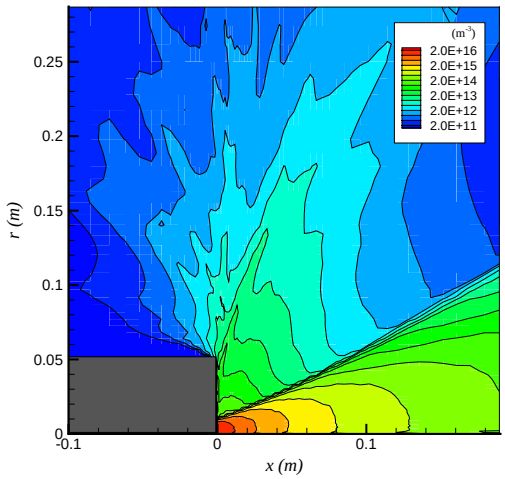

Figure 8. Ion density contours for $T_e = 5.0$ eV.

tion and experiments is also obtained at $\alpha = 20°$, which is not shown here. Hence, $\alpha = 20°$ is chosen as the angle of the ion beam divergence and is applied to the simulations hereafter.

The relation between the plasma potential and electron temperature along the axis is investigated. Figure 6 shows comparisons of the on-axis plasma potential. The potential at the center of the thruster exit plane is obtained from an extrapolation of the experimental data. The computed potential for $T_e = 1.0$ eV is continuously but slowly decreased, whereas a decrease in the potential for $T_e = 5.0$ eV is fairly rapid. On the other hand, the measured potential shows a similar feature up to $x \simeq 0.06$ m to the computed one for $T_e = 5.0$ eV and then it is nearly constant. In the present computation, the electron temperature is assumed to be constant (1.0 or 5.0 eV). However, the electron temperature will be decreased downstream in the plume. Therefore, it is con-

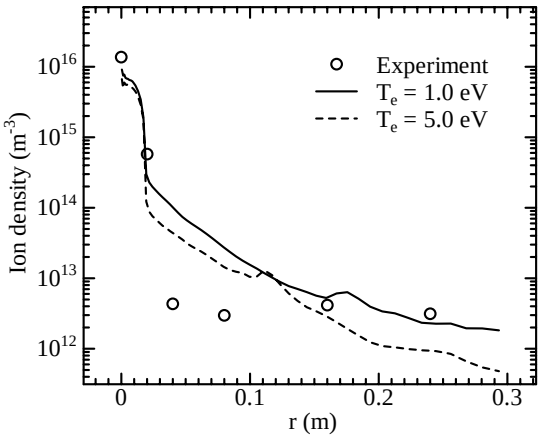

Figure 9. Comparisons of radial ion density at 0.02 m downstream of the thruster exit.

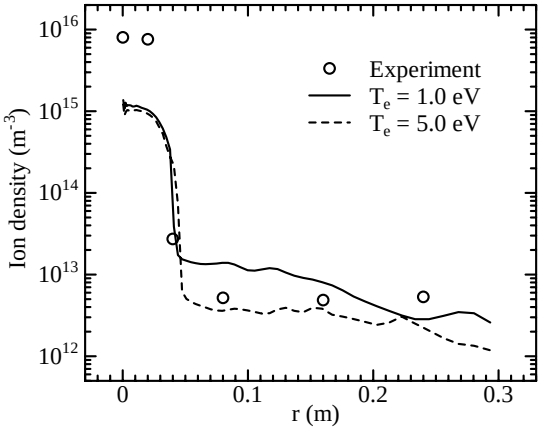

Figure 10. Comparisons of radial ion density at 0.1 m downstream of the thruster exit.

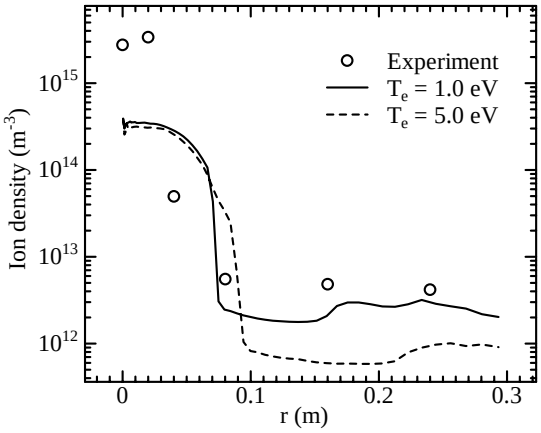

Figure 11. Comparisons of radial ion density at 0.16 m downstream of the thruster exit.

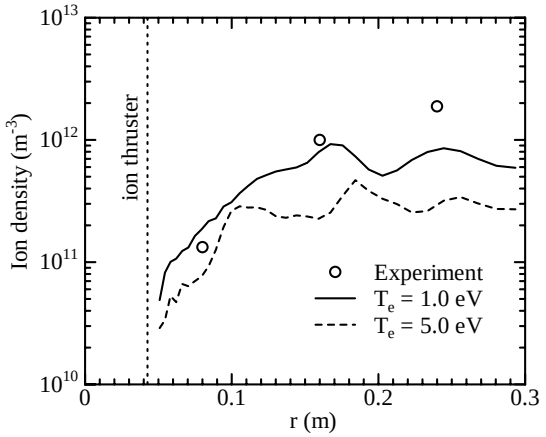

Figure 12. Comparisons of radial ion density at 0.08 m behind the thruster exit.

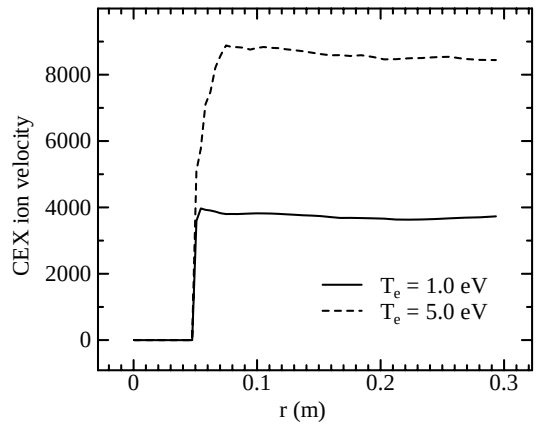

Figure 13. CEX ion velocity at 0.08 m behind the thruster exit.

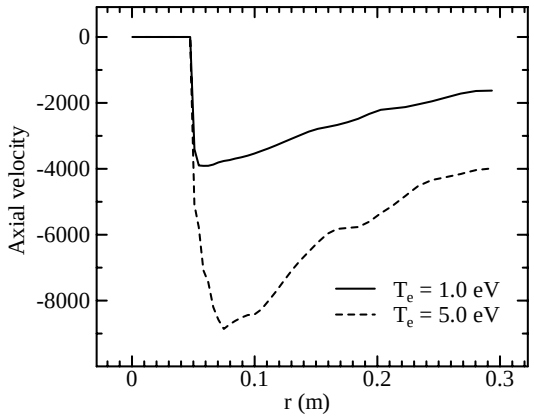

Figure 14. Axial velocity component of CEX ion at 0.08 m behind the thruster exit.

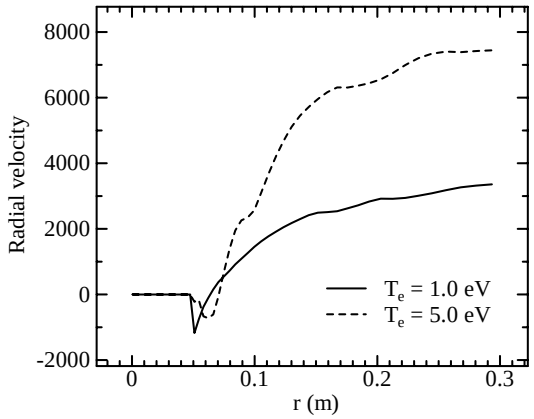

Figure 15. Radial velocity component of CEX ion at 0.08 m behind the thruster exit.

sidered that the measured potential is decreased rapidly in the vicinity of the thruster exit ($x < 0.06$ m) because of high electron temperature, whereas it becomes nearly constant at $x > 0.06$ m because of low electron temperature.

Figures 7 and 8 indicate the ion density contours for T_e = 1.0 and 5.0 eV, respectively. As mentioned earlier, the beam divergence angle has been set to 20°. The CEX ions which are generated by the charge exchange reaction stray out of the beam and are scattered backwards. Figures 7 and 8 show that the ion density within the beam is $2.0 \times 10^{16} - 1.0 \times 10^{14}$ m^{-3}, whereas the CEX ion density outside the beam is $1.0 \times 10^{14} - 2.0 \times 10^{11}$ m^{-3}. These figures also show that the ion beam for T_e = 5.0 eV spreads downstream more widely than that for T_e = 1.0 eV.

The computed results for the radial profile of ion density at 0.02 m downstream of the thruster exit are compared with the experiments in Fig. 9. The density in the ion beam ($0 < r < 0.02$ m) is $1.0 \times 10^{15} - 10^{16}$ m^{-3}. Measured ion density rapidly decreases to 4.0×10^{12} m^{-3} at the beam boundary ($r \simeq 0.02$ m). Outside the beam ($r > 0.02$ m) the measured ion density is nearly constant, whereas the computed results indicate a gradual descend. Although the comparison for different electron temperatures (1.0 and 5.0 eV) gives similar results within the ion beam, the simulated result for T_e = 5.0 eV is slightly smaller than that for T_e = 1.0 eV outside the beam.

Figures 10 and 11 illustrate the radial profiles of ion density at 0.1 m and 0.16 m downstream of the thruster, respectively. In both figures, the computation underpredicts ion density near the axis. As shown in Fig. 11, there is a large discrepancy between the computed results for T_e = 1.0 eV and 5.0 eV outside the beam. The measurements of electron temperature outside the ion beam gives $5 - 10$ eV. Therefore, the comparison between the experiments and simulation for T_e = 5.0 eV indicates

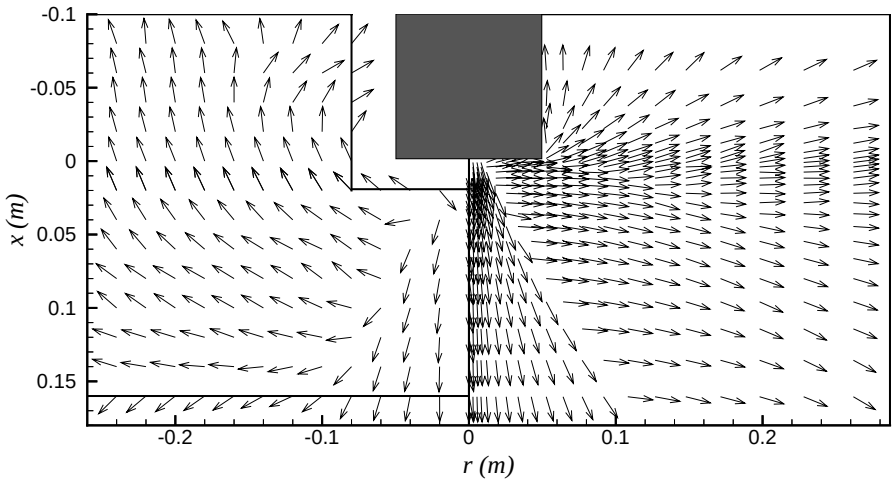

Figure 16. Velocity directions of ion (left: experiment, right: simulation).

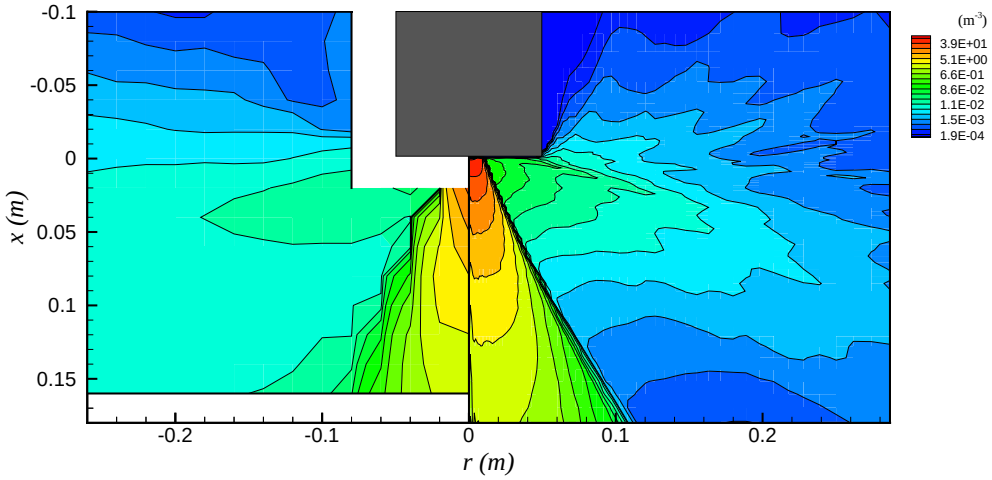

Figure 17. Contours of ion flux (left: experiment, right: simulation).

that the measured CEX ion density is approximately six times as large as the simulation. This discrepancy suggests that the charge exchange cross section in the beam may be higher than that proposed by Rapp and Francis [11].

It is necessary to investigate the behavior of the CEX ions which reach the region behind the ion thruster exit. Figure 12 shows a radial profile of the CEX ions at 0.08 m behind the thruster exit plane. Since the region of $r < 0.05$ m means the ion thruster, no particles exist there. As shown in this figure, the CEX ion density for $T_e = 5.0$ eV is slightly smaller than that for $T_e = 1.0$ eV. The calculated results agree with the experiments near the thruster sidewall.

In Fig. 13, the CEX ion velocity at 0.08 m behind the thruster exit plane are shown for $T_e = 1.0$ eV and 5.0 eV. The CEX ions are accelerated in the backflow region by the electric field. The ion velocity for $T_e = 1.0$ eV is almost constant, $4,000$ m/s, whereas it is approximately $9,000$ m/s for $T_e = 5.0$ eV, which is more than twice as high as that for $T_e = 1.0$ eV. It is apparent that the backflow current is increased because of the higher velocities. Therefore, it is considered that the electron temperature has an effect on the ion thruster plume backflow.

Figures 14 and 15 illustrate the axial and radial velocities of the CEX ions at 0.08 m behind the thruster exit. In both cases, the higher temperature case has a higher velocity than the lower electron temperature case. It can be seen that, away from the axis, the radial velocity component becomes larger than the axial one.

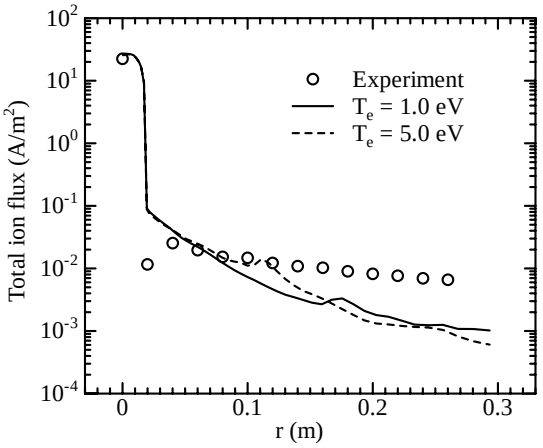

Figure 18. Comparisons of radial ion flux at 0.02 m downstream of the thruster exit.

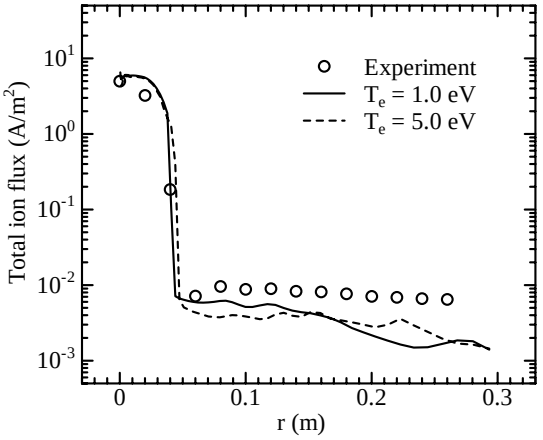

Figure 19. Comparisons of radial ion flux at 0.1 m downstream of the thruster exit.

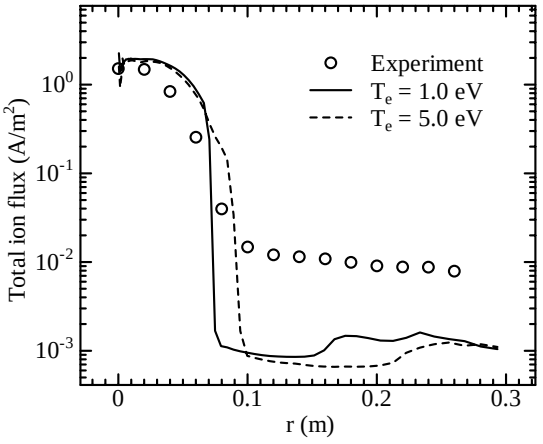

Figure 20. Comparisons of radial ion flux at 0.16 m downstream of the thruster exit.

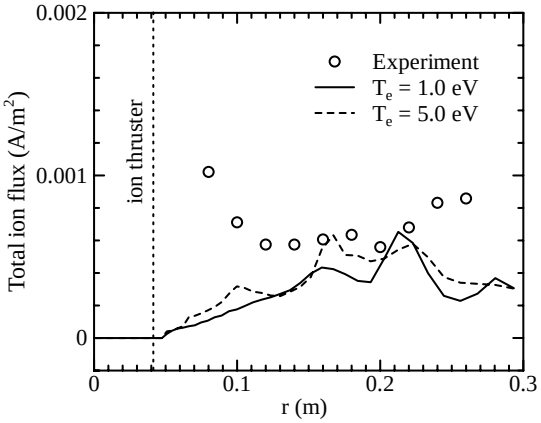

Figure 21. Comparisons of radial ion flux at 0.08 m behind the thruster exit.

Ion velocity directions are demonstrated in Fig. 16. The right indicates the computed result, and the left is the measurements. A discrepancy of velocity directions between the simulation and experiment is seen outside the beam. This suggests that the electron density in the experiments may not be given by the Boltzmann distributions (Eq. (2)) outside the beam.

The simulated total ion flux is compared with the experiment. Figure 17 shows a comparison of the total ion flux contours. The right presents the computed results, and the left is the measurement. A fairly good agreement for the angle of the beam spread is illustrated. As concerns the CEX ions away from the beam, the calculated CEX ion flux is slightly lower than experiments in the downstream region.

Further detailed comparison between the simulation and experiment was conducted. Figure 18 shows the radial profile of the total ion flux at 0.02 m downstream of the thruster exit. The computed results for $T_e = 1.0$ and 5.0 eV show similar features. The computed ion flux is gradually decreased away from the beam whereas the measurement shows only an appreciable decrease.

The results at 0.1 m and 0.16 m downstream of the exit are presented in Figs. 19 and 20, respectively. A good agreement between the simulation and experiment is shown within the ion beam in Fig. 19. On the other hand, the computed CEX ion flux outside the beam is slightly smaller than the measured one. As shown in Fig. 20, the difference between the computed and measured CEX ion fluxes outside the beam is large compared with that inside the beam. This is presumably because the actual charge exchange cross section may become higher than that proposed by Rapp and Francis, as away from the ion thruster exit. Figure 21 shows the comparisons of the ion fluxes at 0.08 m behind the thruster exit.

Conclusions

The DSMC-PIC method was applied to numerically simulate the plume from a small size ion thruster and especially to reveal the behavior of the CEX ions. The present computational procedure is such that first of all, the density and velocity of neutral atoms are calculated beforehand using the DSMC method and then the simulation of the ion beam is carried out by using the DSMC-PIC method.

The simulated results for the ion flux, plasma potential and density were compared with experiments conducted at ISAS. By comparing the computed and measured on-axis ion fluxes, a good agreement is obtained for the ion beam spread angle $\alpha = 20°$. A comparison of the on-axis plasma potential suggests that the constant electron temperature in the beam is not adequate. The higher electron temperature causes the ion beam spread and an increase in the CEX ion velocity in the backflow region. A discrepancy of velocity directions between the simulation and experiment is seen outside the beam, because electron density may not be satisfied with the Boltzmann distribution. Further improvements of the simulation model in the backflow region are needed. Comparison of the CEX ion flux indicates that the charge exchange cross section within the beam becomes higher than the theoretical value as away from the ion thruster exit.

References

[1] K. Toki, H. Kuninaka, I. Funai, K. Nishiyama and Y. Shimizu, "Development Status of a Microwave Ion Engine System for the MUSES-C Mission," 26th Int. Electric Propulsion Conf., Kitakyushu, Japan, IEPC-99-139, Oct. 1999.

[2] H. Kuninaka, I. Funaki, K. Nishiyama, P. Molina-Morales and Y. Nakayama, "Virtual Anode Phenomana Due to Lack of Neutralization on Ion Thrusters Based on MUSES-C Program," AIAA-2001-3785, 2001.

[3] R.I. Samanta Roy, "Numerical Simulation of Ion Thruster Plume Backflow for Spacecraft Contamination Assessment," Ph.D thesis, MIT, 1995

[4] R.I. Samanta Roy, D.E. Hastings and N.A. Gatsonis, "Numerical Study of Spacecraft Contamination and Interactions by Ion-Thruster Effluents," *Journal of Spacecraft and Rockets* **33**, *535-542*, 1996.

[5] R.I. Samanta Roy and D.E. Hastings, "Ion-Thruster Plume Modeling for Backflow Contamination," *Journal of Spacecraft and Rockets* **33**, *524-534*, 1996.

[6] C.K. Birdsall and A.B. Langdon, Plasma Physics Via Computer Simulation, Adam Hilger, 1991.

[7] J. Wang and J. Brophy, "3-D Monte-Carlo Particle-in-Cell Simulations of Ion Thruster Plasma Interactions," AIAA Paper 95-2826, 1995

[8] J. Wang, J. Brophy and D. Brinza, "3-D Simulations of NSTAR Ion Thruster Plasma Environment," AIAA Paper 96-3202, 1996

[9] D.B. van Gilder, G.I. Font and I.D. Boyd, "Hybrid Monte Carlo-Particle-in-Cell Simulation of an Ion Thruster Plume," *Journal of Propulsion and Power* **15**, *530-538*, 1999.

[10] G.A. Bird, Molecular Gas Dynamics and the Direct Simulation of Gas Flows, Clarendon Press, Oxford, England, 1994.

[11] Rapp and W.E. Francis, "Charge Exchange Between Gaseous Ions and Atoms," *Journal of Chemical Physics* **37**, *2631-2645*, 1962.